Acta Crystallographica Section D
**Biological Crystallography**
ISSN 0907-4449

# Thaumatin crystallization aboard the International Space Station using liquid–liquid diffusion in the Enhanced Gaseous Nitrogen Dewar (EGN)

**Cindy L. Barnes,[a] Edward H. Snell[a] and Craig E. Kundrot[b]***

[a]Mail Code SD46, Marshall Space Flight Center, AL 35812, USA, and [b]Mail Code SD41, Marshall Space Flight Center, AL 35812, USA

Correspondence e-mail: craig.kundrot@msfc.nasa.gov

Received 20 November 2001
Accepted 8 February 2002

This paper reports results from the first biological crystal-growth experiment on the International Space Station (ISS). Crystals of thaumatin were grown using liquid–liquid diffusion in Tygon® tubing transported in the Enhanced Gaseous Nitrogen Dewar (EGN). Different volume ratios and concentrations of protein and precipitant were used to test different adaptations of the vapor-diffusion crystallization recipe to the liquid–liquid diffusion method. The EGN warmed up from 77 to 273 K in about 4 d, about the same time it took to warm from 273 to 293 K. The temperature within the EGN was 293–297 K for the majority of the experiment. Air gaps that blocked liquid–liquid diffusion formed in the tubes. Nonetheless, crystals were grown. Synchrotron diffraction data collected from the best space-grown crystal extended to 1.28 Å, comparable to previous studies of space-grown thaumatin crystals. The resolution of the best ground-control crystal was only 1.47 Å. It is not clear if the difference in diffraction limit arises from factors other than crystal size. Improvements in temperature control and the elimination of air gaps are needed, but the results show that the EGN on the ISS can be used to produce space-grown crystals that diffract to high resolution.

## 1. Introduction

During the assembly of the International Space Station (ISS), NASA's biological crystal-growth program is switching from an emphasis on using the Space Shuttle Orbiter to an emphasis on using the ISS. The primary advantages of the ISS are that it provides the opportunity for longer periods of weightlessness (1–3 months on ISS *versus* 1–2 weeks on the Orbiter) and dedicated facilities that can be used regularly. This paper reports results from the first biological crystal-growth experiment on the ISS.

In the period 1985–2000, NASA flew 45 biological crystal-growth missions in space, primarily on the Space Shuttle Orbiter. About 35% of the proteins, nucleic acids and viruses that flew more than once produced crystals with better diffraction limits than any previously terrestrially grown crystal (Kundrot *et al.*, 2001). Only five of the 45 missions were dedicated to conducting microgravity experiments. Most of the missions had a primary purpose that was detrimental for growing crystals in a low-acceleration environment, *e.g.* launching satellites from the Orbiter cargo bay.

Eight missions delivered experiments to the Russian space station Mir.

Two crystallization methods were developed for the Mir environment: the Gaseous Nitrogen Dewar (GN2; Koszelak *et al.*, 1996) and the Diffusion-controlled Crystallization Appa-

© 2002 International Union of Crystallography
Printed in Denmark – all rights reserved

ratus for Microgravity (DCAM; Carter *et al.*, 1999). The biological crystallization experiments performed on Mir were subject to the operational constraints of no crew involvement and no electrical power. Both methods are passive and employ liquid–liquid diffusion. The DCAM contains a 50 µl microdialysis button in direct contact with a 2 ml reservoir that is connected in turn to a 8 ml reservoir *via* an exchangeable gel plug of varying dimensions. Equilibration between the large reservoir and the microdialysis button requires weeks or months. The GN2, on the other hand, is based on the free-interface diffusion technique (Salemme, 1972, 1985; Zeppezauer *et al.*, 1968). The unique aspect of the GN2 is that the solutions are first frozen on the ground and later thawed in space. The thawing initiates the crystallization. The GN2 uses a Dewar that is charged with 12 l of liquid nitrogen before transporting the experiments to orbit. In a typical configuration, the GN2 holds about 500 segments of Tygon® tubing, about 3 mm in outer diameter and 85 mm long, that are sealed at each end. Each tube contains about 150 µl of frozen solution. For batch crystallization, the frozen solution is one homogeneous solution (Fig. 1). For liquid–liquid diffusion crystallization, one half of the tubing is typically filled with a solution containing the crystallization target and the other half is filled with a precipitant. After the Dewar is delivered to the space station and the nitrogen boils off, the samples melt and warm up to the ambient temperature. When the solutions melt, diffusive mixing takes place (Garcia Ruiz *et al.*, 1999). In addition to requiring no crew time or power, the GN2 can carry a large number of samples, has no moving parts and is very tolerant of launch delays. The apparatus used in this work, the Enhanced Gaseous Nitrogen Dewar (EGN), is a slightly modified version of the GN2. The EGN has the added capability of measuring and recording the temperature within the Dewar throughout the mission.

There are two major advantages to conducting liquid–liquid diffusion experiments in orbit compared with on the ground. Firstly, the buoyancy-driven convection between the different density slugs in the tube is severely reduced on orbiting platforms. To some extent, convective mixing can be minimized on the ground by orienting the apparatus so that less dense solutions are always above more dense solutions. The problem remains, however, that a growing crystal will sediment away from its nucleation site to the bottom of the tube. The second benefit of the weightless environment of space is that crystal sedimentation is severely reduced. On the ground,

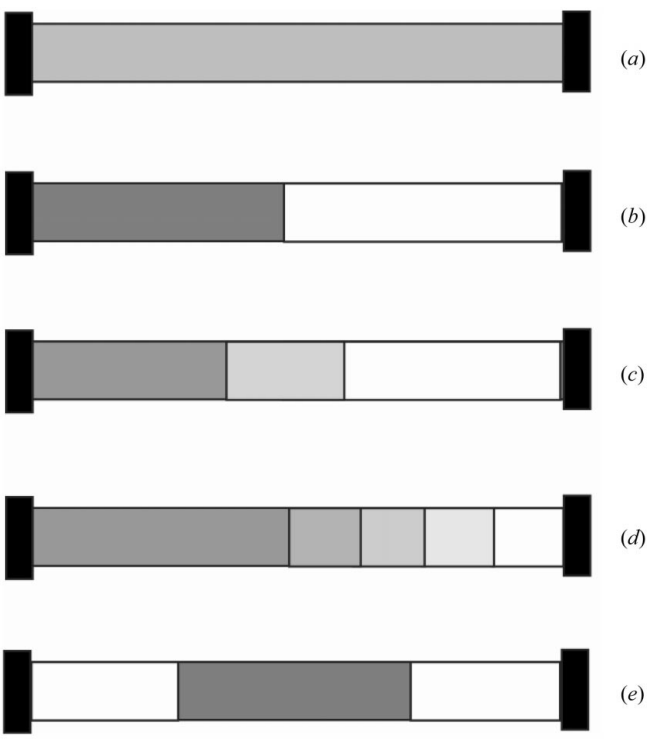


**Figure 1**
Arrangements of solutions in tubing (after Koszelak *et al.*, 1996). (*a*) Uniform (batch), (*b*) two-phase, (*c*) three-phase, (*d*) sequential step gradient, (*e*) double interface. The tubes used in this study were 1.6 × ~85 mm and enclosed a volume of about 170 µl.

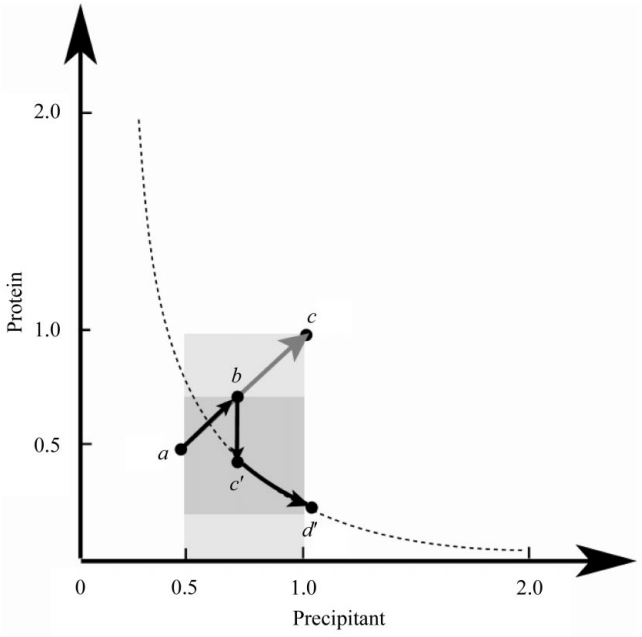


**Figure 2**
The standard hanging-drop experiment. The arrows show the trajectory of the hanging drop with respect to the protein solubility curve in the phase diagram as the drop equilibrates. It is assumed that the hanging drop is a homogeneous solution and that the effects of the solutes in the protein solution upon the activity of water are negligible compared with the effect of the solutes in the precipitant solution. Equal volumes of protein and precipitant solution, each at 1.0× concentration, are added together to form the initial drop. Both the protein and the precipitant are therefore initially at 0.5× concentration (point *a*). The gray arrow depicts the case where the protein remains in solution. Water evaporates from the drop until the 1× concentration of the precipitant is restored (point *c*). The black arrows depict the case where the protein comes out of solution. The trajectory crosses the solubility curve and enters a metastable region. Upon nucleation of crystal growth (or precipitate formation) (point *b*), the trajectory shows a sharp decrease in the protein concentration as it drops to the solubility curve (point *c*′). The trajectory then moves along the solubility curve until the final precipitant concentration is reached (point *d*′). *A priori*, the trajectory is confined to the gray-shaded region. The darker gray region shows the limits actually attained in the experiment.

sedimentation can be arrested by a gel network or by a dialysis membrane (Ducruix & Giegé, 1992; Robert *et al.*, 1992). However, gels often perturb the crystallization experiment and membranes limit the distance the crystals sediment rather than prevent sedimentation. The reduced convection and sedimentation in space support the formation of a much larger depletion zone around the growing crystal (Kam *et al.*, 1978; Otálora *et al.*, 2001). The depletion zone reduces the speed of crystal growth and may allow a more perfect lattice to be formed.

The aim of the work reported here was to explore different ways of adapting terrestrial hanging-drop vapor-diffusion crystallization recipes for use with the EGN on the ISS. The protein thaumatin was chosen as a model system because of its previous crystallization in space (Lorber *et al.*, 1999, 2000; Ng *et al.*, 1997) and previous studies of its growth mechanism (Kuznetsov *et al.*, 1999; Malkin *et al.*, 1996, 1999). Previous diffraction studies of thaumatin have reported diffraction resolution of 1.65–1.75 Å for crystals grown by vapor diffusion on the ground (Ko *et al.*, 1994; Ogata *et al.*, 1992) and 1.2–1.5 Å resolution for crystals grown in space by liquid–liquid diffusion in the Advanced Protein Crystallization Facility space flight hardware (Lorber *et al.*, 1999; Ng *et al.*, 1997). The space-grown crystals grown in this study diffracted to 1.28–1.37 Å resolution, compared with 1.47–1.52 Å for the ground-control crystals.

## 2. Experimental

### 2.1. Experimental design

These experiments were designed to use the EGN in a way that mimics crystallization conditions experienced in ground-based vapor-diffusion experiments. More specifically, the trajectory of the EGN experiment in a phase diagram was designed in terms of the trajectory followed in the ground-based vapor-diffusion experiment (Fig. 2).

The simplest adaptation of a hanging-drop crystallization recipe for free-interface diffusion is the 'half-and-half' recipe (Koszelak *et al.*, 1996). In this approach, half the liquid volume is protein and half is precipitant. The concentrations of the precipitant and protein solutions are double the concentration of their final concentrations in the vapor-diffusion experiment. When the solution is completely mixed, the final concentrations are the same as the final concentrations in the vapor-diffusion trajectory. This 'half-and-half' recipe results in a trajectory that is far outside the region of the vapor-diffusion region (Fig. 3). The protein solution located near the protein–precipitant interface, for example, will be exposed to 2× precipitant concentration before it returns to the final equilibrium value of 1×.

Three series of tubes were set up to explore alternatives to the 'half-and-half' formulation (Table 1). The first series was designed to minimize the high precipitant concentrations that

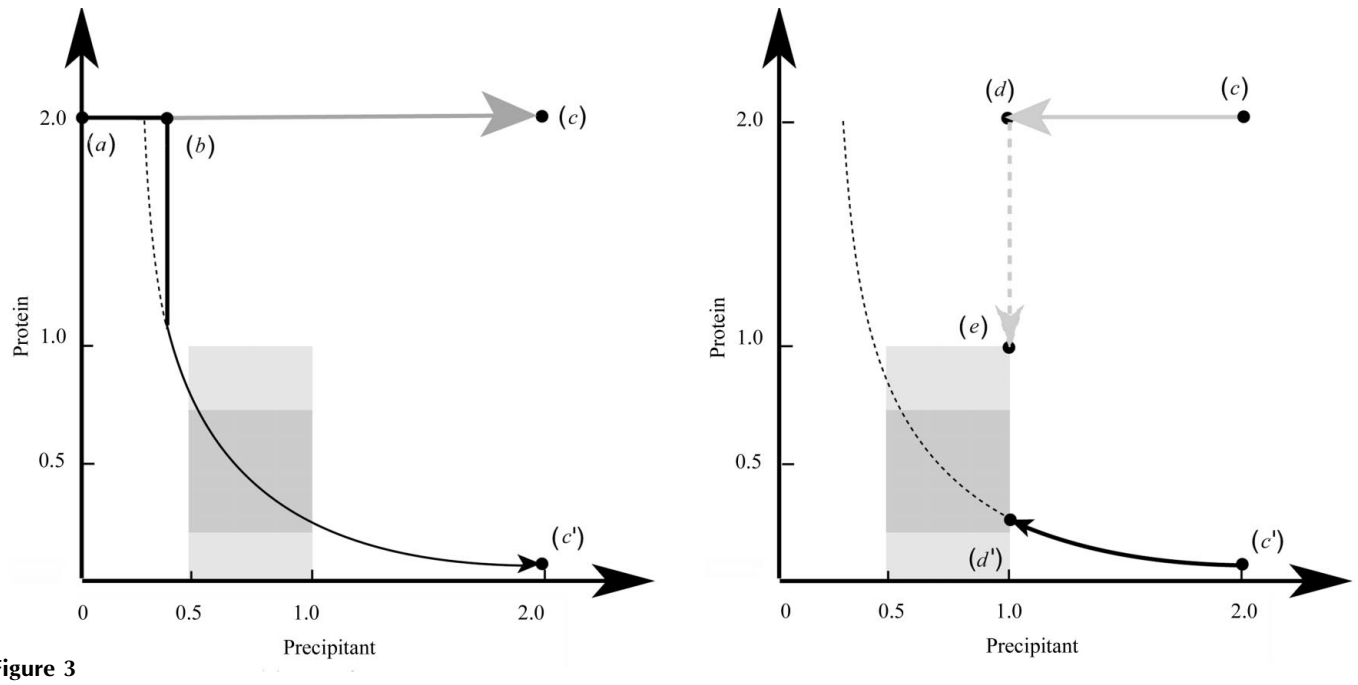


**Figure 3**
The 'half-and-half' free-interface diffusion experiment. The trajectories are shown for a point in the protein solution that is very near the protein–precipitant interface. The protein diffusion into the precipitant is assumed to be negligible. The gray arrows depict the case where protein remains in solution. The trajectory begins at zero precipitant concentration (point *a*) and rises to essentially undiluted initial precipitant concentration (point *c*). As the precipitant continues to diffuse into the protein region, the precipitant concentration drops until it reaches 1× precipitant concentration (point *d*). If the protein is also allowed to redistribute throughout the tube (*e.g.* over a long time scale or with active mixing), the trajectory reaches the same point as the final vapor-diffusion experiment (point *e*). The black arrows show the trajectory taken when protein crystallization/precipitation occurs. The trajectory begins as before at point *a* and as the precipitant concentration increases the protein eventually crystallizes or precipitates (point *b*). As the concentration of precipitant climbs, the trajectory moves along the solubility curve, passes through the final equilibration point and reaches 2× precipitant concentration (point *c*′). Lastly, as the precipitant solution is diluted into the protein region, the trajectory retraces the solubility curve to arrive at the final equilibrium point (point *d*′). Positions in the tube that are further removed from the protein–precipitant interface will have similar trajectories but the overshoot beyond 1× precipitant concentration will be less.

develop in the protein solution. This series was a reference series in that it kept the *final* concentrations of protein and precipitant in the fully mixed tube approximately constant. The variables in this series (compared with the 'half-and-half' recipe) were the *initial* precipitant and protein volumes (and, by extension, their initial concentrations). The initial precipitant volume was increased so that the precipitant concentration would be reduced compared with the 'half-and-half' formulation. The initial protein volume was decreased by the corresponding amount while keeping the amount of protein constant.

This first series sampled trajectories quite different to the trajectories in hanging-drop vapor-diffusion experiments and the 'half-and-half' formulation. Compared with the 'half-and-half' formulation depicted in Fig. 3, the larger the initial precipitant solution was, the less the trajectory would overshoot the 1× precipitant value. However, the reduction of the protein volume forced the trajectory to begin at protein concentrations higher than 2×. The second series of tubes was intended to ameliorate the potential problems associated with higher protein concentrations while retaining the benefit of lower precipitant concentrations.

The second series repeated the volume fractions of the first series, but fixed the initial protein concentrations at 1×, *i.e.*, the final concentration expected in the vapor-diffusion experiments. Compared with the 'half-and-half' formulation depicted in Fig. 3, the tubes with a small volume fraction of protein had a reduced precipitant overshoot as in the first series, but the trajectories in this series began from only 1× protein concentration.

The third series incorporated two modifications relative to the second series. One modification was to prevent the protein and precipitant solutions from mixing during loading or at low temperatures. When protein solution is added to a tube containing frozen precipitant solution, some of the precipitant solution may thaw and mix with the protein solution. Also, the two solutions will thaw at around 273 K and there may be substantial mixing of the solutions before the EGN warms to ambient temperatures (*e.g.* 295 K). Therefore, a 10 µl slug of buffer was placed in between the protein and precipitant. This slug effectively acts as a fuse that delays the mixing of protein and precipitant until the solutions have warmed further. The other modification was intended to minimize the possibility of crystals forming and then later dissolving. A small amount of protein was also added to the precipitant solution to decrease the amount of crystal dissolution that occurs when the tubing contents are thoroughly mixed and the crystals must be in equilibrium with the total volume of the tubing.

**Table 1**
Tubing contents.

| | | | | Initial | | | | | Final† |
|---|---|---|---|---|---|---|---|---|---|
| | | | | Thaumatin | | Tartrate | | Tartrate plus thaumatin‡ | Thaumatin |
| Series | Tube ID | Crystal | Protein volume fraction | Conc. (mg ml$^{-1}$) | Vol. (µl) | Conc. (*M*)§ | Vol. (µl) | Vol. (µl) | Conc. (mg ml$^{-1}$) |
| 1 | HOA | $\mu$1, $\mu$2 | 0.38 | 39 | 53 | 1.60 | 87 | | 15 |
| | HOB | | 0.38 | 39 | 53 | 1.60 | 87 | | 15 |
| | HOC | | 0.32 | 45 | 45 | 1.47 | 95 | | 14 |
| | HOD | | 0.32 | 45 | 45 | 1.47 | 95 | | 14 |
| | HOE | | 0.26 | 59 | 36 | 1.35 | 104 | | 15 |
| | HOF | | 0.26 | 59 | 36 | 1.35 | 104 | | 15 |
| | HOG | | 0.20 | 87 | 28 | 1.25 | 112 | | 17 |
| | HOH | $\mu$3 | 0.20 | 87 | 28 | 1.25 | 112 | | 17 |
| | HOI | | 0.14 | 132 | 20 | 1.16 | 120 | | 19 |
| | HOJ | | 0.14 | 132 | 20 | 1.16 | 120 | | 19 |
| | IKG¶ | $\mu$4 | 0.10 | 162 | 14 | 1.11 | 126 | | 16 |
| 2 | HOK | | 0.38 | 15 | 53 | 1.60 | 87 | | 5.7 |
| | HOL | | 0.38 | 15 | 53 | 1.60 | 87 | | 5.7 |
| | HOM | | 0.32 | 15 | 45 | 1.47 | 95 | | 4.8 |
| | HON | | 0.32 | 15 | 45 | 1.47 | 95 | | 4.8 |
| | HOO | G1, G2 | 0.26 | 15 | 36 | 1.35 | 104 | | 3.9 |
| | HOP | | 0.26 | 15 | 36 | 1.35 | 104 | | 3.9 |
| | HOQ | | 0.20 | 15 | 28 | 1.25 | 112 | | 3.0 |
| | HOR | | 0.20 | 15 | 28 | 1.25 | 112 | | 3.0 |
| | HOS | | 0.14 | 15 | 20 | 1.16 | 120 | | 2.1 |
| | HOT | | 0.14 | 15 | 20 | 1.16 | 120 | | 2.1 |
| 3 | HOU | | 0.38 | 15 | 53 | 1.60 | 10 | 77 | 5.9 |
| | HOV | | 0.38 | 15 | 53 | 1.60 | 10 | 77 | 5.9 |
| | HOW | | 0.32 | 15 | 45 | 1.47 | 10 | 85 | 5.1 |
| | HOX | | 0.32 | 15 | 45 | 1.47 | 10 | 85 | 5.1 |
| | HOY | | 0.26 | 15 | 36 | 1.35 | 10 | 94 | 4.2 |
| | HOZ | | 0.26 | 15 | 36 | 1.35 | 10 | 94 | 4.2 |
| | HPA | | 0.20 | 15 | 28 | 1.25 | 10 | 102 | 3.4 |
| | HPB | | 0.20 | 15 | 28 | 1.25 | 10 | 102 | 3.4 |
| | HPC | | 0.14 | 15 | 20 | 1.16 | 10 | 110 | 2.5 |
| | HPD | | 0.14 | 15 | 20 | 1.16 | 10 | 110 | 2.5 |

† The final concentration of sodium potassium tartrate was 1.0 *M* for all tubes. § Tartrate solutions also contained 100 m*M* ADA pH 6.5. ‡ 0.5 mg ml$^{-1}$ thaumatin. ¶ Conditions used in a subsequent flight experiment from STS-98 (ISS assembly flight 5A, February 2001) to STS-102 (ISS assembly flight 5A.1, March 2001) testing the reproducibility of the results. Note: STS flight numbers are not chronological.

### 2.2. Crystallization

Tygon® S-50-HL tubing of 3.2 mm outer diameter and 1.6 mm inner diameter was used to contain the crystallization solutions. All solutions were degassed for 15 min prior to loading. Thaumatin from Sigma (Lot 108F0299) was dissolved in degassed doubly distilled water. A 12 cm length of tubing was held in a U shape and loaded with precipitant solution (Table 1). The tube was sealed 1.75 cm from the end with a SEBRA (Tucson, AZ) Model 1105 Tube Sealer. Any air bubbles in the sample were removed by swinging the sample rapidly downward by hand. The precipitant solution was frozen by dipping 0.5–1 cm of the crimped end of the tubing in and out of liquid nitrogen several times. Once the solution in the tubing began to freeze, the entire tube was immersed in the liquid nitrogen until all of the solution froze. The tube was removed from the liquid nitrogen and protein was added using a Hamilton syringe. The tubing was immersed

in liquid nitrogen until the protein solution froze and was then sealed about 1.75 cm from the end of the tubing. Frozen tubes were stored at 193 K until EGN loading. Samples were inspected for tube cracking twice prior to being loaded in the EGN. The inspections briefly exposed the samples to 277 or 295 K, but no observable melting of the tube contents occurred during the inspection.

### 2.3. Flight

The samples were loaded in the EGN on 7 September 2000 and launched on STS-106 (ISS assembly flight 2A.2B) on 8 September 2000. The EGN was transferred to the FGB section of the ISS on 13 September 2000 and stowed behind panel number 312. NASA has not provided the orientation of the EGN with respect to the ISS, so the direction of the residual acceleration with respect to the crystallization experiments is unknown. The EGN was transferred to an Orbiter, STS-92 (ISS assembly flight 3A) on 18 October (note: NASA flight designations do not follow chronological order). The Orbiter undocked from ISS on 20 October 2000 and landed at Edwards Air Force Base on 24 October 2000, 46 d after EGN was launched. Samples were unloaded from EGN at University of California-Irvine on 26 October 2000 and distributed to the investigators on 27 October 2000.

Ground controls were prepared as follows. Tubes were loaded in the same manner as the tubes that flew in the EGN. After the temperature data were available from this first flight of the EGN, conditions were selected for thawing the ground-control tubes. It was not possible to mimic the temperature *versus* time profile of the EGN throughout the entire temperature range (*i.e.* from 77 to 293 K) using commonly available laboratory equipment. Therefore, we selected an arrangement that most closely duplicated the warming kinetics in the 273–293 K range, as this is the temperature region in which the precipitant and protein solutions in the tubes thaw and begin to mix. A Taylor–Wharton 10 l LD Dewar was filled with 500 g of ice and 500 ml of liquid nitrogen. The ground-control samples were placed in 50 ml conical tubes to keep them dry and laid horizontally in the Dewar. A Fluke 51 K/J thermometer with a K-type thermocouple probe was inserted through a Stryofoam cap that covered the end of the Dewar. The Dewar was kept in a horizontal orientation. The Dewar warmed up from 84 to 276.0 K in 20 h and from 276.0 to 293.4 K in 45 h.

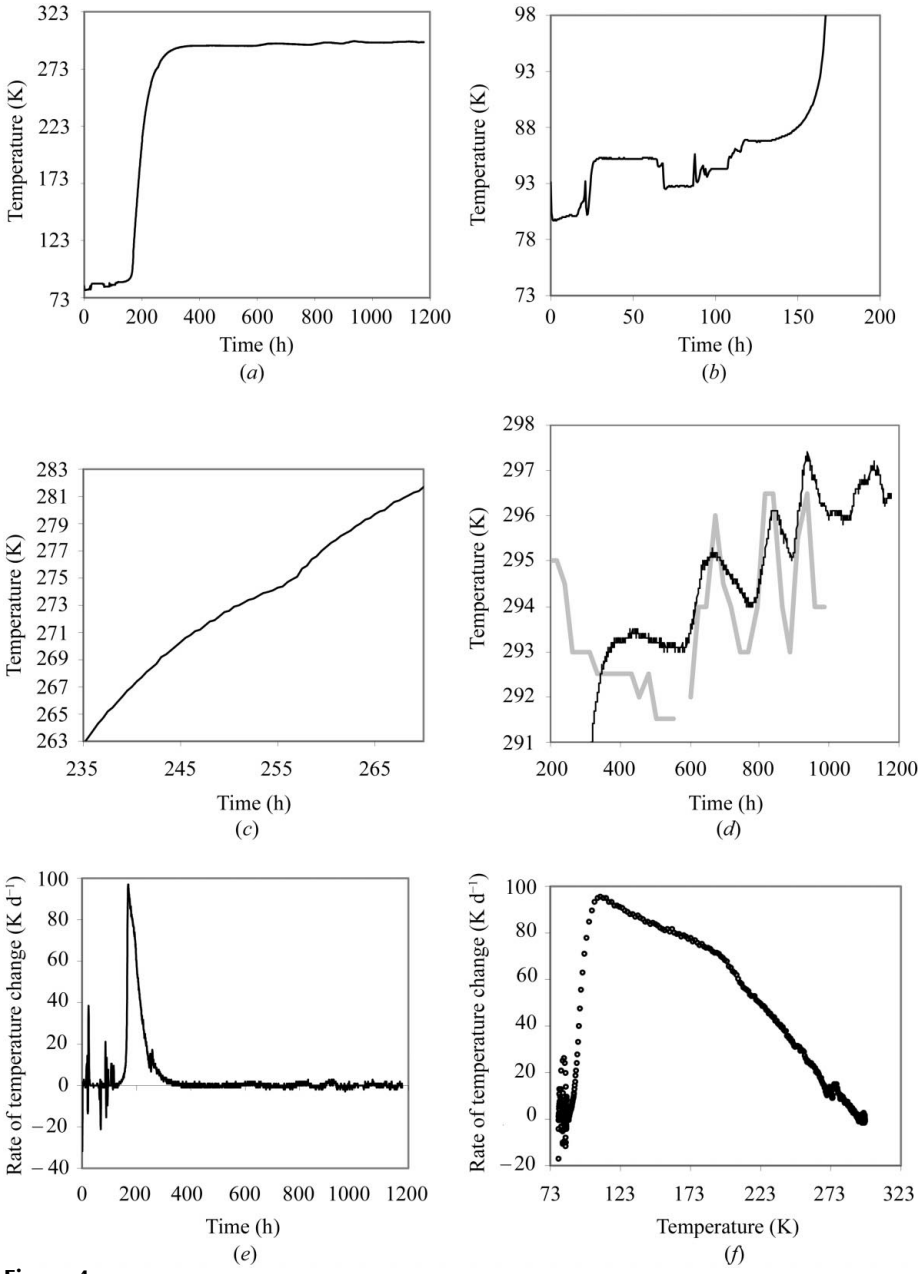


**Figure 4**
The temperature profile of the EGN from the time of loading the EGN for flight 2A.3b through the recovery of the EGN from flight 3A. The temperature *versus* time is shown for the complete mission in (*a*), the nitrogen boil-off phase in (*b*), melting in (*c*) and the ambient period in (*d*) (EGN temperature in black, median daily cabin temperature in gray). Zero time is the time at which the EGN was loaded. The derivatives of the temperature change with respect to time and temperature are shown in (*e*) and (*f*), respectively.

### 2.4. X-ray crystallography

Three crystals were studied at beamline 7-1 of the Stanford Synchrotron Radiation Laboratory 14 d after their return to Earth. The crystals were mounted in quartz glass capillaries

with plugs of mother liquor sealed with epoxy resin and nail polish. Crystals $\mu$1 and $\mu$2 from experiment ID HOA were mounted in the laboratory 24 h before the experiment. Crystal $\mu$3 from experiment ID HOH was mounted just prior to the experiment. The crystals were bipyramidal in shape and were measured at their longest and thickest dimensions. Microgravity has been shown to dramatically reduce the mosaicity of crystals (Borgstahl *et al.*, 2001; Ng *et al.*, 1997; Snell *et al.*, 1995, 2001), so data were collected at 295 K to maintain the physical perfection and deconvolute possible effects of cryocooling. A wavelength of 1.08 Å was used with a MAR 345 imaging-plate detector and the beam was collimated to 100 × 100 µm. The protocol for data collection was a high-resolution slow scan using the full detector at 120 mm distance, with 40 images of 1° oscillation in dose mode, equivalent to a 30 s exposure at the start of the experiment. This was followed by a coarse low-resolution fast scan, with 180 mm of the detector, 20 images, 2° oscillations and an exposure time equal to a 9 s exposure at the start of the experiment. If any decay in the images was seen, the crystals were large enough to allow translation. To initiate each experiment, a single image was used to index the crystal with *MOSFLM* (Leslie, 1992) and to obtain a data-collection strategy to maximize the completeness of the resulting data. The strategy adopted was to divide the data collection into two equal swathes of 20° of reciprocal space each to maximize the possible data completeness. Crystals $\mu$1 and $\mu$3 both required contiguous 40° swathes; crystal $\mu$2 required two 20° swathes, 90° apart.

On a subsequent synchrotron run, data were collected from two ground-control samples, G1 and G2, from experiment ID HOO (Table 1) on the same beamline using identical protocols with the same detector and X-ray dose as used for $\mu$1, $\mu$2 and $\mu$3. An additional microgravity crystal, $\mu$4, from a separate ISS mission [STS-98 (ISS assembly flight 5A) to STS-102 (ISS assembly flight 5A.1)], experiment ID IKG, was also studied with 20 images of 1° oscillation and ten of 2° oscillation owing to beamtime constraints. For crystal G1 the maximum completeness data set was obtained with two 20° swathes 55° apart while for crystal G2 two 20° swathes 40° apart were needed.

## 3. Results and discussion

### 3.1. Temperature profile of EGN

The EGN temperature profile contains three stages of interest: (i) nitrogen boil-off, (ii) warm-up to ambient and (iii) ambient (Fig. 4). In the first stage, changes in cabin pressure change the boiling point of liquid nitrogen (Fig. 4*b*). These temperature variations are not expected to have an effect on the crystallization since all the solutions are frozen.

In the second stage, the warming is relatively rapid from 77 to 273 K but slow from 273 to 293 K (Figs. 4*c*, 4*e* and 4*f*). The maximum warming rate occurs shortly after the liquid nitrogen boils off and is about 100 K d$^{-1}$. The warming rate steadily decreases with increasing temperature and at about 199 K the warming rate falls more rapidly with increasing temperature. This temperature, 199 K, is 50–70 K higher than the glass transitions of water or protein crystals (Weik *et al.*, 2001). The transitions from 93 to 193 K and 193 to 253 K both took 30 h. The transition from 253 to 274 K was similar, 26 h. However, the final warming from 273 to 293 K required 110 h. This long equilibration time is presumably primarily because of the small temperature gradient. The larger heat capacity of the liquid solutions compared with the frozen solutions may also have slowed the equilibration rate. Once in the ambient range, the temperature of the EGN changed at a rate of less than 3 K d$^{-1}$ (Fig. 4*d*). The temperature changes of the EGN correlate with the fluctuations of the ISS cabin temperature.

The slow warming between the melting and ambient temperatures could have large effects on the crystallization process. The protein and precipitant solutions will generally have different melting points and will melt at different times. This difference in melting times appears to affect where bubbles form in the tubes (see §3.2). During the 100 h of warming from 273 to 293 K, a significant amount of diffusion of tartrate into the protein solution can take place. Tartrate has a diffusion coefficient of the order of $10^{-5}$ cm$^2$ s$^{-1}$, so in 100 h the root-mean diffusion distance of tartrate will be almost 3 cm, close to the half the length of the tubing. Some nucleation and crystallization of protein is therefore possible at temperatures below ambient and the selection of crystallization targets for EGN should consider this fact.

Once having achieved ambient temperature, there are significant temperature fluctuations of the order of a day (*i.e.* 3 K d$^{-1}$). This level of temperature fluctuation may be unacceptable for many macromolecular crystallizations.

### 3.2. Air gaps

Surprisingly, all the sample tubes flown in the EGN contained bubbles that spanned the internal diameter of the tubing, *i.e.* air gaps. There were 3–7 air gaps per tube, with an average of 4.8 air gaps per tube (standard deviation of 1.2).

The location of the air gaps 4 d after unloading is depicted in Fig. 5. 29 of the 30 tubes had an air gap at that end of the

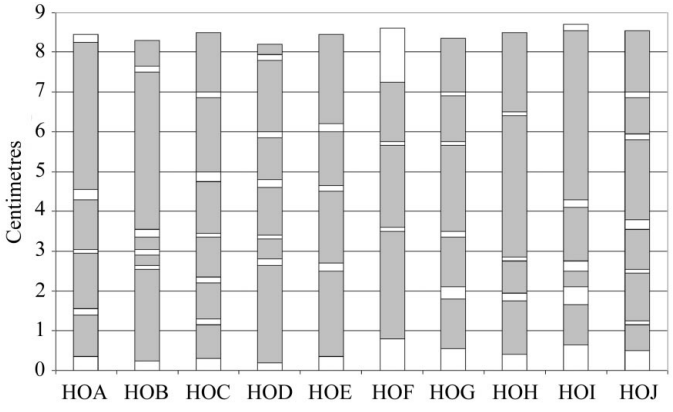


**Figure 5**
Location of air gaps for series 1. Air gaps (white) and liquid slugs (gray) are depicted. Protein and precipitant solutions were initially at the bottom and the top of the tube, respectively.

**Table 2**
X-ray data metrics.

The slow high-resolution, fast low-resolution and combined data sets are presented. Values in parentheses are for the highest resolution shell.

| | | Wilson plot | | Unit-cell parameters (Å) | | | | | | | |
|---|---|---|---|---|---|---|---|---|---|---|---|
| Crystal | Size | Scale factor | *B* factor | $a = b$ | $c$ | Resolution (Å) | *R* factor | $I/\sigma$ | Completeness (%) | Unique reflections | Mosaicity (°) |
| $\mu$1 | 0.97 × 0.57 × 0.46 | 1.34 | 13.0 | 58.56 | 151.58 | | | | | | |
| Slow | | | | | | 40–1.2 | 9.8 (60.1) | 14.2 (1.3) | 64.7 (46.1) | 54106 | 0.122 |
| Fast | | | | | | 40–1.9 | 5.1 (48.1) | 10.7 (2.2) | 42.7 (35.6) | 9270 | 1.633 |
| Combined | | | | | | 40–1.2 | 7.4 (60.1) | 13.9 (1.3) | 74.3 (47.3) | 61964 | 0.170 |
| $\mu$2 | 0.91 × 0.47 × 0.44 | 1.18 | 13.4 | 58.53 | 151.59 | | | | | | |
| Slow | | | | | | 40–1.2 | 7.3 (57.1) | 17.3 (1.5) | 85.2 (74.5) | 71094 | 0.106 |
| Fast | | | | | | 40–1.9 | 5.7 (13.0) | 17.2 (7.2) | 70.1 (91.1) | 15176 | 0.113 |
| Combined | | | | | | 40–1.2 | 8.0 (59.0) | 17.5 (1.4) | 89.3 (78.2) | 74394 | 0.105 |
| $\mu$3 | 1.97 × 1.00 × 1.00 | 1.00 | 15.3 | 58.50 | 151.63 | | | | | | |
| Slow | | | | | | 40–1.2 | 6.8 (39.0) | 17.6 (1.4) | 83.6 (49.3) | 69528 | 0.090 |
| Fast | | | | | | 40–1.9 | 5.2 (10.6) | 23.9 (11.2) | 86.5 (98.8) | 18758 | 0.097 |
| Combined | | | | | | 40–1.2 | 6.9 (39.0) | 23.8 (1.4) | 90.2 (49.3) | 75042 | 0.091 |
| $\mu$4 | 0.75 × 0.34 × 0.16 | 1.85 | 13.9 | 58.56 | 151.37 | | | | | | |
| Slow | | | | | | 40–1.2 | 4.7 (39.4) | 17.9 (1.4) | 72.3 (24.3) | 60201 | 0.148 |
| Fast | | | | | | 40–1.9 | 3.5 (8.6) | 18.4 (7.2) | 55.0 (76.6) | 11916 | 0.201 |
| Combined | | | | | | 40–1.2 | 5.9 (39.3) | 17.8 (1.3) | 72.8 (26.1) | 60585 | 0.157 |
| G1 | 0.24 × 0.16 × 0.16 | 4.37 | 15.7 | 58.49 | 151.42 | | | | | | |
| Slow | | | | | | 40–1.4 | 5.5 (53.3) | 16.8 (1.2) | 89.8 (62.5) | 47499 | 0.102 |
| Fast | | | | | | 40–1.9 | 10.0 (85.3) | 8.7 (1.1) | 87.7 (86.4) | 18987 | 0.199 |
| Combined | | | | | | 20–1.4 | 13.9 (55.6) | 18.6 (1.3) | 90.7 (67.3) | 47897 | 0.111 |
| G2 | 0.34 × 0.18 × 0.18 | 3.05 | 14.5 | 58.52 | 151.42 | | | | | | |
| Slow | | | | | | 40–1.3 | 7.4 (62.9) | 17.1 (1.1) | 85.7 (37.8) | 56326 | 0.118 |
| Fast | | | | | | 40–1.9 | 11.5 (61.7) | 11.2 (1.8) | 91.5 (98.1) | 196843 | 0.317 |
| Combined | | | | | | 40–1.3 | 15.0 (62.6) | 17.5 (1.1) | 86.6 (37.7) | 56926 | 0.137 |

tubing which was loaded with protein. About 70% of the air-gap volume was located in the protein solution part of the tubing. The total air-gap volume for series 1 (Table 1) measured on 30 October (4 d after unloading) ranged from 9 to 27% (mean = 14%, standard deviation = 5%) of the total tube volume.

Additional air gaps formed in the tubes after return to Earth. These air gaps were produced from pre-existing bubbles as water evaporated from the tubes. Sample tubes stored in a 295 K incubator lost 1.1–1.4 mg of mass per day depending on the relative humidity of the air in the incubator. Ground-control experiments with tubes partially filled with water showed a similar rate of mass loss that was, to a first approximation, independent of the volume of the tube filled with water. On average, five new air gaps per tube were formed in between the 6th and 53rd day after flight.

The presence of the air gaps upon sample return to Earth indicated that the intended liquid–liquid diffusion experiment did not occur in orbit. Each bubble that forms slows the mass transport through the tubing. Air gaps block the liquid–liquid diffusion process entirely, while still allowing vapor diffusion across the air gap. Smaller bubbles that did not span the internal diameter of the tubing were also present in the EGN tubes. Such bubbles alter the equilibration kinetics by decreasing the cross-sectional area available for liquid–liquid diffusion. In addition to altering the equilibration kinetics, the location and time of formation of bubbles cannot be exactly replicated. Such crystallization experiments are therefore not reproducible.

There appear to be two processes that create the air gaps. The melting of the protein and precipitant solutions initially produces air gaps. The 85 cm tubing can hold about 170 µl of liquid. However, the freezing of the tubing in liquid nitrogen is slow enough that the solution expands as it freezes. Only about 140 µl of liquid can be accommodated after it is frozen if the tube is kept open during freezing. Therefore, when the solid melts, the volume of the tubing contents decreases from 170 µl of solid to 140 µl of liquid. The difference of 30 µl leads to the formation of air gaps in the tubing. Other samples prepared by sealing both ends of the tubing prior to freezing also exhibited air gaps (A. McPherson, personal communication).

Evaporative loss of water (and other volatile components) through the tubing also produces air gaps by allowing existing bubbles to grow. In orbit, all the samples are enclosed in a sealed cylinder. Since the water activity of the samples in the cylinder differ, water may be exchanged between tubes *via* the vapor phase. Ground experiments show that tubes containing 3 *M* NaCl solution in contact with moistened Kim-Wipes gain about 0.27 mg per day. So, after thawing, some tubes in the EGN cylinder may lose water and some may gain water. After the EGN is returned to Earth and the cylinder is opened, however, all tubes begin to lose water through this evaporative process.

Subsequent ground experiments have shown two simple ways of preventing air-gap formation. The first is to crimp both ends of the tubing before the final freezing step. This is the standard method used by McPherson, Koszelak and collea-

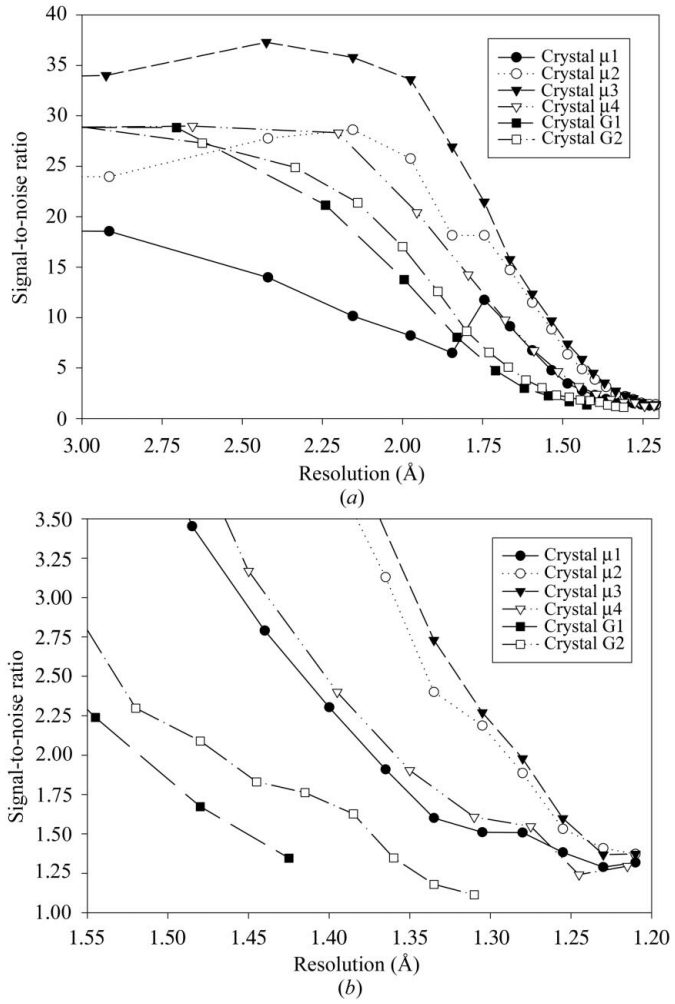


**Figure 6**
Diffraction data. (*a*) Plot of signal to noise against resolution for all crystal samples from 3.0 Å to the maximum resolution of the data set. Each point represents the midpoint of the resolution bin for the data. (*b*) Magnified region between 1.55 Å and the resolution limit.

gues. It reduces the number of air gaps formed, but does not eliminate them entirely. The principal drawback of crimping both ends before freezing is that full tubes often burst during the freezing process and therefore cannot be loaded into EGN. The second remedy is to fill the tube partially rather than completely. The partially filling of the tube also ameliorates the problem of crimping both ends of the tubing prior to freezing by providing room for the expansion of the solid. Smaller sample volumes are also more conducive to structural biology investigations that have limited quantities of the target being crystallized.

Despite the formation of air gaps and bubbles, this series of crystallization experiments produced crystals that diffract to a comparable resolution to thaumatin crystals grown with different apparatus in agarose gel using the dialysis method on a previous microgravity mission (Lorber *et al.*, 1999).

### 3.3. Synchrotron results

The data were integrated using *DENZO* and reduced with *SCALEPACK* (Otwinowski & Minor, 1997). The results are summarized in Table 2. Crystal $\mu$3 provided a good data set to 1.28 Å at the $2I/\sigma$ level and these data together with extra data collected on that crystal are being used for structural refinement. Crystal $\mu$1 decayed rapidly in the X-ray beam, as can be seen by comparison of the low-resolution pass with that of the other two crystals. The large mosaic spread seen for the fast scan of crystal $\mu$1 is a consequence of radiation damage from the previous slow-scan data collection. The decay prompted a 50 µm translation after the first 20 images. During the fast collection of crystal $\mu$2 the beam was lost and the fast data set had to be restarted after a refill. Crystal $\mu$3 did not show radiation decay after the first 20 images but was translated by 100 µm to preempt any that might occur.

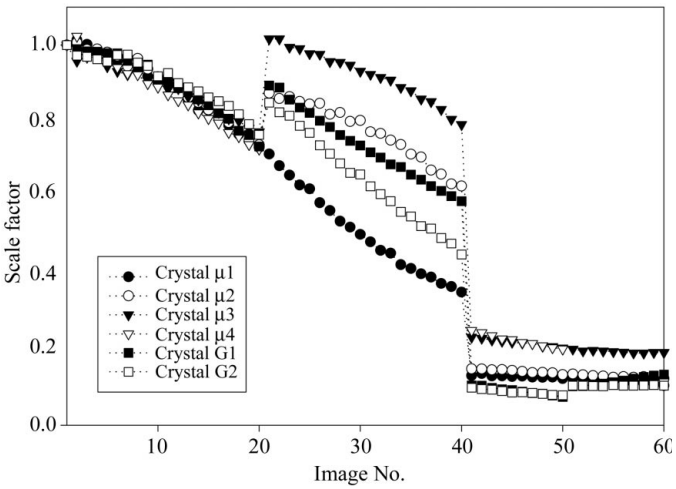


**Figure 7**
Plot of the scale factor obtained from *SCALEPACK* (Otwinowski & Minor, 1997) against the image number. The scale factor has been normalized to the first image. Clearly illustrated is the data-collection protocol of a slow high-resolution pass in the first 40 images followed by a quick low-resolution pass for the final 20 images. All microgravity crystals except $\mu$1 were translated in the beam after image 20 was collected. Crystal $\mu$4 had a reduced data collection as described in the text.

The ground crystals G1 and G2 diffracted to lower resolutions of 1.52 and 1.47 Å for G1 and G2 at the $2I/\sigma$ level, respectively. The ground crystals were smaller than the microgravity crystals and, given the beam size, could not be translated to minimize radiation-damage effects.

Fig. 6 shows plots of the signal to noise of the data from the crystals from 3 Å in Fig. 6(*a*) and the high-resolution region enlarged in Fig. 6(*b*). The general trend is for the microgravity crystals to show improved signal to noise throughout, with the exception of $\mu$1 which clearly shows the radiation decay in the low-resolution fast-pass data set. Looking at the high-resolution data (Fig. 6*b*), it becomes clear that the microgravity crystals diffract more strongly: this is not an unexpected result given the illuminated volume differences.

Fig. 7 plots the scale factor for each image based on normalizing to the first image in each data set. The scale factor corrects for X-ray beam decay and radiation effects in the crystal. Because dose mode was used throughout for each sample, we can neglect the effects of beam decay as each image resulted from a comparable number of X-ray photons. Once care has been taken that the error model for each crystal

is accurate, the reduction in scale factor arises entirely from the crystal decay. Esposito *et al.* (1998) noted reduced X-ray radiation in their microgravity samples compared with their earth-grown crystals. In Fig. 7 this would be evidenced by different gradients. There is not a discernible difference in this case. Fig. 7 is also interesting from a data-collection standpoint. It is clear that collecting two swathes of data separated by a number of degrees provides better data. It is even clearer, and common knowledge, that translation of a crystal is beneficial to a good data set. Crystal $\mu$1 suffered from significant radiation decay and it seems that this may have been prevented had the crystal been translated, as in the case of crystal $\mu$3.

The microgravity crystals appear better in every metric examined, with higher resolution, signal to noise, improved $R$ factor and completeness. Mosaicity has been seen to dramatically improve in microgravity (Borgstahl *et al.*, 2001; Ng *et al.*, 1997; Snell *et al.*, 1995, 2001). The values presented here, however, show no clear trends. This is not surprising as the mosaicity is a convolution of instrumental, spectral and geometric effects (Bellamy *et al.*, 2000) with the mosaicity of the crystal. The beamline used, 7-1, focuses the X-ray radiation, hence the mosaicities noted in Table 2 mask those of the crystal.

The reason for the improvement in diffraction resolution from the space-grown crystals is unclear. The space-grown crystals were larger but the 100 µm square synchrotron beam was smaller than the crystal cross sections so only the depth of the crystal illuminated by the X-ray beam differed between crystals. The linear dimensions of the space-grown crystals are six to nine times larger than the earth-grown crystals. The scale factor between $\mu$3 and G1 is 4.36 (Table 2). Therefore, the illuminated volume is one contribution. Ideally, crystals of the same volume from both space and ground populations should be used for a strict comparison. This option was not available to us as the microgravity crystals were consistently larger than the ground controls. The crystal order, as measured by Wilson plots, does not appear to be different between space-grown and earth-grown crystals; the $B$ factors for all crystals are in the range 13.0–15.7 Å$^2$. One other source of improvement could arise from reduced background levels in the space-grown crystals, which could be caused by reduction in long-range disorder that produces diffuse scatter near the Bragg peak.

### 3.4. Extensions of the method

Many extensions to the EGN method presented here are possible. The experiments described in this work are the first steps in one approach toward adapting vapor-diffusion recipes for free-interface diffusion. Additional refinements can be made to make the free-interface diffusion trajectory coincide more closely with the vapor-diffusion trajectory. The protein solution could contain precipitant, but in an amount that keeps the protein soluble throughout the EGN temperature range, *i.e.* between 273 and 303 K. Similarly, the precipitant solution could contain a subsaturating amount of protein solution. It is important that the solution be subsaturating at ambient temperatures, but if the precipitation of the protein at lower temperatures is reversible, precipitation at low temperatures is probably acceptable. In general, there is a need to strike a balance between two mutually exclusive choices in this approach: (i) create the same endpoint as the ground-based vapor-diffusion conditions or (ii) stay within the envelope of vapor-diffusion precipitant conditions.

In some cases, however, it may be desirable for the free-interface diffusion trajectory to be quite different from the vapor-diffusion trajectory. One example is the crystallization of complexes. To crystallize the complex $A$–$B$, it may be desirable to have one solution containing $A$ and a second solution containing $B$ so that crystallization will occur at the interface of the solutions.

## 4. Conclusions

The EGN used on ISS has several limitations, but produces high diffraction quality protein crystals. The slow warming of the crystallization tubes (warming from 273 to 293 K takes about 4 d) must be considered in the choice of crystallization target and the arrangement of protein, precipitant and buffer slugs in the crystallization tube. The temperature environment for this flight of EGN was too variable for many crystallization systems. After initially warming to 293 K, the EGN underwent periodic temperature variations that were superimposed on a generally upward trend. The peak temperature was over 297 K. The second limitation was the formation of air gaps and bubbles in the crystallization tubes that blocked or retarded liquid–liquid diffusion. The time and location of air-gap formation is not known and is unpredictable. The air gaps prevented the original intent of the experiment (testing the effect of different volume ratios and concentrations of protein and precipitant on the liquid–liquid diffusion method) from being carried out. Despite these limitations, thaumatin crystals grown in the EGN diffracted to higher resolution than ground-control crystals. It appears worthwhile then to refine the use of EGN on ISS to provide a robust method of growing crystals of a wide range of proteins, nucleic acids, viruses and complexes.

CLB and EHS are contracted to NASA through the Universities Space Research Association. We thank A. McPherson for the opportunity to fly samples in the EGN. We thank S. Koszelak, J. Ng, M. Myers, G. Jenkins and J. Perkey for advice on how to load tubes and for their operational support of the EGN flight, J. Vernon for sample preparation, J. Wilks for post-flight analysis and G. Borgstahl, J. A. Gavira and M. van der Woerd for synchrotron time and assistance with data collection. This work is based upon research conducted at the Stanford Synchrotron Radiation Laboratory (SSRL), which is funded by the Department of Energy (BES, BER) and the National Institutes of Health (NCRR, NIGMS). This work was funded by NASA Research Announcement awards to CEK and G. Borgstahl and by NASA Macromolecular Biotechnology Discipline Science Funds.

## References


Bellamy, H. D., Snell, E. H., Lovelace, J., Pokross, M. & Borgstahl, G. E. (2000). *Acta Cryst.* D**56**, 986–995.

Borgstahl, G. E. O., Vahedi-Fardi, A., Lovelace, J., Bellamy, H. & Snell, E. H. (2001). *Acta Cryst.* D**57**, 1204–1207.

Carter, D. C., Wright, B., Miller, T., Chapman, J., Twigg, P., Keeling, K., Moody, K., White, M., Click, J., Ruble, J. R., Ho, J. X., Adcock-Downey, L., Bunick, G. & Harp, J. (1999). *J. Cryst. Growth*, **196**, 602–609.

Ducruix, A. & Giegé, R. (1992). *Crystallization of Nucleic Acids and Proteins: A Practical Approach*, edited by A. Ducruix & R. Giegé, pp. 73–98. New York: IRL Press.

Esposito, L., Sica, F., Sorrentino, G., Berisio, R., Carotenuto, L., Giordano, A., Raia, C. A., Rossi, M., Lamzin, V. S., Wilson, K. S. & Zagari, A. (1998). *Acta Cryst.* D**54**, 386–390.

Garcia Ruiz, J. M., Novella, M. L. & Otálora, F. (1999). *J. Cryst. Growth*, **196**, 703–710.

Kam, Z., Shore, H. B. & Feher, G. (1978). *J. Mol. Biol.* **123**, 539–555.

Ko, T. P., Day, J., Greenwood, A. & McPherson, A. (1994). *Acta Cryst.* D**50**, 813–825.

Koszelak, S., Leja, C., & McPherson, A. (1996). *Biotechnol. Bioeng.* **52**, 449–458.

Kundrot, C. E., Judge, R. A., Pusey, M. L. & Snell, E. H. (2001). *Cryst. Growth Des.* **1**, 87–99.

Kuznetsov, Y. G., Malkin, A. J. & McPherson, A. (1999). *J. Cryst. Growth*, **196**, 489–502.

Leslie, A. G. W. (1992). *Jnt CCP4/ESF–EAMCB Newsl. Protein Crystallogr.* **26**.

Lorber, B., Ng, J. D., Lautenschlager, P. & Giegé, R. (2000). *J. Cryst. Growth*, **208,** 665–677.

Lorber, B., Sauter, C., Robert, M. C., Capelle, B. & Giegé, R. (1999). *Acta Cryst.* D**55**, 1491–1494.

Malkin, A. J., Kuznetsov, Y. G., Glantz, W. & McPherson, A. (1996). *J. Phys. Chem.* **100**, 11736–11743.

Malkin, A. J., Kuznetsov, Y. G. & McPherson, A. (1999). *J. Cryst. Growth*, **196**, 471–488.

Ng, J. D., Lorber, B., Giegé, R., Koszelak, S., Day, J., Greenwood, A. & McPherson, A. (1997). *Acta Cryst.* D**53**, 724–733.

Ogata, C. M., Gordon, P. F., de Vos, A. M. & Kim, S.-H. (1992). *J. Mol. Biol.* **228**, 893–908.

Otálora, F., Novella, M. L., Gavira, J. A., Thomas, B. R. & Garcia Ruiz, J. M. (2001). *Acta Cryst.* D**57**, 412–417.

Otwinowski, Z. & Minor, W. (1997). *Methods Enzymol.* **276**, 307–326.

Robert, M. C., Provost, K. & LeFaucheux, F. (1992). *Crystallization of Nucleic Acids and Proteins: A Practical Approach*, edited by A. Ducruix & R. Giegé, pp. 127–143. New York: IRL Press.

Salemme, F. R. (1972). *Arch. Biochem. Biophys.* **151**, 533–539.

Salemme, F. R. (1985). *Methods Enzymol.* **114**, 140–141.

Snell, E. H., Judge, R. A., Crawford, L., Forsythe, E. L., Pusey, M. L., Sportiello, M., Todd, P., Bellamy, H., Lovelace, J., Cassanto, J. M. & Borgstahl, G. E. O. (2001). *Cryst. Growth Des.* **1**, 151–158.

Snell, E. H., Weisgerber, S., Helliwell, J. R., Weckert, E., Hölzer, K. & Schroer, K. (1995). *Acta Cryst.* D**51**, 1099–1102.

Weik, M., Ravelli, R. B., Silman, I., Sussman, J. L., Gros, P. & Kroon, J. (2001). *Protein Sci.* **10**, 1953–1961.

Zeppezauer, M., Eklund, H. & Zeppezauer, E. S. (1968). *Arch. Biochem. Biophys.* **126**, 564–573.